JOURNAL OF GUIDANCE, CONTROL, AND DYNAMICS
Vol. 19, No. 3, May–June 1996

Adaptive Orbit Determination for Interplanetary Spacecraft

P. Daniel Burkhart*
Jet Propulsion Laboratory, California Institute of Technology, Pasadena, California 91109
and
Robert H. Bishop†
University of Texas at Austin, Austin, Texas 78712

The interplanetary orbit determination problem has been traditionally solved using least-squares techniques. Because of the operational limitations of this method, a Kalman filter approach has been proposed for future missions that includes all spacecraft and measurement modeling states in the filter. The goal is to increase the accuracy of the navigation process while utilizing only radiometric (Doppler and range) data. As an extension, an adaptive orbit determination approach (based on the Magill filter bank) has been developed here to process radiometric data. This adaptive approach can be used to systematically determine the operational filter parameters, which are currently selected using ad hoc methods. The Mars Pathfinder mission is utilized to demonstrate the effectiveness of the adaptive filter bank in determining variances for the process and measurement noise parameters based on the tracking data. Error budgets are presented for the range and Doppler cases, which show nongravitational accelerations and solar radiation pressure to be the main error sources. Results for the range case show that the adaptive enhanced filter bank is effective in selecting the noise variances that match those used to generate the data. Results for the Doppler case are not as conclusive, resulting primarily from linearization errors.

I. Introduction

THE orbit determination problem for interplanetary spacecraft involves the calculation of spacecraft states (i.e., position and velocity) and associated estimation uncertainty measures based on information received from measurements that are corrupted by various errors and random noise. One problem with the current approach to solving this problem is the lack of a systematic method for determining appropriate values for the operational orbit determination filter. The operational filter parameters, such as time constants, gravitational parameters, noise variances and system parameters, are generally selected by trial and error based on experience and computer simulation. A set of filter parameters is selected and the measurement data are processed. Based on the simulation results, the filter parameters may be changed and the data processed again, or the current result may be accepted. During this iterative process, often the measurement data are deweighted, resulting in estimation errors that are generally higher than the data requires. This ad hoc approach to filter tuning, in addition to failing to take full advantage of the inherent data accuracy, requires a large number of navigation team members to analyze the results. Despite the success of this approach in the past, current realities do not support its continued use. The orbit determination task must be completed with fewer analysts because of reductions in resources for navigation, similar if not greater tracking accuracy requirements, and less tracking data.

In addition to the systematic tuning of the operational filter, an approach for detecting environmental changes is desirable. Suppose the process noise and/or data noise profile changes during the mission. For example, the acceleration profile of the spacecraft may change significantly as a result of unmodeled venting. The need for a non-labor-intensive method to detect changes in the data profile and to point to the source of the changes is clear (e.g., detect an unmodeled vent).

Received June 19, 1995; revision received Dec. 8, 1995; accepted for publication Dec. 19, 1995.

*Member, Technical Staff, Navigation and Flight Mechanics Section. Member AIAA.
†Associate Professor, Department of Aerospace Engineering and Engineering Mechanics. Member AIAA.

For these reasons, a new orbit determination methodology is desirable for operational interplanetary navigation. The motivation for the work presented here is to improve the operational tools used to perform the interplanetary orbit determination function.

One constraint on the proposed solution is the utilization of realistic error sources and realistic models to accurately determine whether the proposed approach will be useful in an operational environment. In addition, the proposed solution must integrate easily with current navigation approaches. Since a Kalman filter approach will be used for future interplanetary missions, the solution must be compatible with this recursive filter method. Because of the desire to minimize tracking station use, personnel costs, and complexity, only conventional Doppler and ranging data will be considered. Finally, the proposed solution must be implementable in a modular fashion. This is not only to avoid extensive modification of existing orbit determination software, but also to allow testing and verification in a smoother and less complicated fashion.

Along with the change from the least-squares filter to the Kalman filter, another major change in the current filtering practice is reflected in the so-called enhanced filter.[1] Current practice involves modeling certain Earth platform and transmission media effects as consider parameters in the filter. In other words, these parameters are allowed to affect the covariance of the estimated state, but are not themselves estimated. The enhanced filter calls for inclusion of all of these parameters in the estimated state vector. In other words, the enhanced filter has no consider parameters. When compared with current filtering practices, the result is increased accuracy in the state estimates.[1] This filtering strategy is currently being tested using actual flight data from Galileo.[2] The enhanced Kalman filter is utilized in this paper.

The scenario chosen for this study is the Mars Pathfinder mission, scheduled for launch in December 1996. Specifics of the mission plan, including launch and arrival dates and the tracking scenario, are presented. A model was developed to represent accurately, but with moderate complexity, the actual data received by the filter during a mission. This model, consisting of the spacecraft state, solar radiation pressure effects, small unmodeled acceleration effects, transmission media effects, and Earth platform effects, is used to generate tracking data.

The approach taken here is to utilize radiometric (Doppler and range) data and to establish navigation improvements through the use of adaptive filtering algorithms. Several methods were investigated in terms of ability to determine both process noise and

measurement noise parameters and to be general enough to handle a time-varying problem. Since the Kalman filter is already in use and is planned for future use for orbit determination, a method utilizing this approach is desirable for implementation reasons. It was found that the most desirable approach, in terms of these constraints, is the Magill Kalman filter bank,[3] also known as the multiple model estimation algorithm (MMEA).

All of the adaptive filtering approaches increase in computational cost as the number of filter parameters to be determined increases. For this reason, it is desirable to determine only the most critical error sources and to concentrate effort in the analysis on these areas. The less significant errors will remain as parameters in the filter, but will not participate in the adaptation. A special type of covariance analysis, or error budget analysis, is utilized here to catalog the contributions of particular error sources or error source groups to the overall estimation error. The error budget is presented for X-band range only and Doppler-only measurement scenarios for the Mars Pathfinder mission.

Results are given for several different sets of noise parameters included in the adaptive scheme. The main result is the demonstrated ability of the adaptive Kalman filter bank to determine the underlying measurement and process noise strengths. In addition, the results for the changing noise strengths case show the ability of the filter bank to detect environmental and/or spacecraft changes.

Following this introduction is the Mars Pathfinder mission description in Sec. II, with the covariance analysis description next in Sec. III. Section IV details adaptive filtering approaches and the Kalman filter bank. The simulation results are presented in Sec. V, followed by conclusions and future directions in Sec. VI.

II. Mars Pathfinder Mission

The Mars Pathfinder mission is the first of a series of low-cost rapid turnaround science missions from NASA's Discovery Program. This mission will serve primarily as a demonstration of key technologies and concepts for use in future missions to Mars using scientific landers. In addition, Pathfinder includes a significant science payload. Investigations of the Martian atmosphere, surface meteorology, surface geology and morphology, and elemental composition of Martian rocks and soil are scheduled for Pathfinder. A free-ranging surface microrover is also part of the mission. This microrover will be deployed by Pathfinder to conduct technology related experiments and to serve as a mechanism for instrument deployment.[4]

The mission is scheduled for the 1996 Mars launch opportunity, with a 30-day launch window beginning on Dec. 5, 1996, and ending on Jan. 3, 1997. The arrival date at Mars is fixed at July 4, 1997. The transfer time will vary from 212 to 182 days, depending on the actual launch date. The trajectory used for this study corresponds to the Jan. 3, 1997, launch date. Upon arrival at Mars on July 4, 1997, the spacecraft will perform a direct entry into the Martian atmosphere. To achieve a landing, a parachute is deployed along with a rocket braking system and an airbag system. After landing, the primary surface operations begin, which includes deployment of the microrover.[4]

The interplanetary transfer phase of the Mars Pathfinder mission is under investigation here. The adaptive filtering approach proposed for the interplanetary navigation problem is not dependent on the Mars Pathfinder mission. The Mars Pathfinder scenario is chosen so that the adaptive filtering method can be tested using a realistic interplanetary mission. Epoch conditions are known for the spacecraft and the planets on March 5, 1997. The data arc used in this study lasts for 105 days from the epoch, or until June 18, 1997. A plot of the Earth, spacecraft, and Mars trajectories is shown in Fig. 1. The trajectory characteristics (the shaded portion of Fig. 1) are detailed in Table 1. During interplanetary cruise, the scientific instruments will be checked but not used.

The interplanetary cruise portion of the mission begins approximately 7 days after launch (L + 7) and ends 15 days before encounter (M − 15). The main task during interplanetary cruise is to determine the required corrections to the trajectory to ensure the spacecraft arrives when and where it is scheduled. The nominal mission plan has four trajectory correction maneuvers (TCMs), if required. The first

Table 1 Mars Pathfinder trajectory characteristics (March 5–June 18, 1997)

Parameter	Value (start to end of arc)
Earth to spacecraft range, km	36.2×10^6 to 180×10^6
Geocentric declination, deg	15.85 to −0.12
Sun–Earth-probe angle, deg	1.4 to 51.7

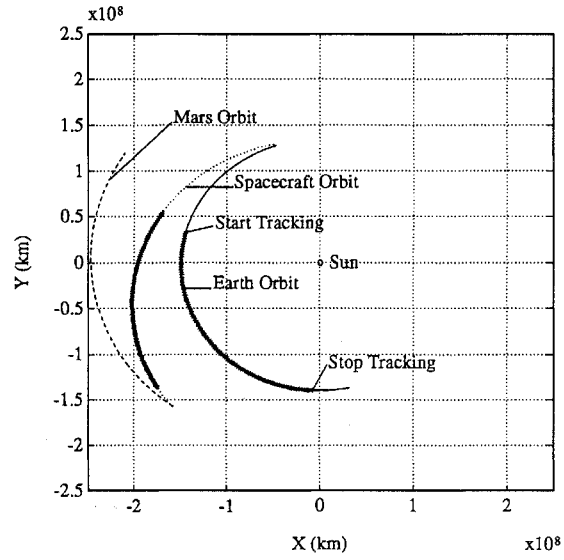

Fig. 1 Mars Pathfinder trajectory (planar projection).

two maneuvers are scheduled at L + 30 days (to correct for injection errors) and L + 60 days (to correct remaining injection errors and TCM 1 errors). The third maneuver is scheduled for M − 60 days (for entry targeting), whereas the final maneuver is planned for M − 10 days (to ensure the landing conditions are met). Thus the data arc used here begins after the completion of the first two TCMs and will include the third TCM. The solution at the end of data processing will be propagated to encounter, which includes the fourth TCM. The navigation solution, obtained after processing the data from the 105-day interplanetary cruise, will be used to support the final TCM if the maneuver is required. The errors resulting from the fourth TCM will not affect the navigation solution significantly.[4]

The tracking scenario contains two-way X/X band data taken from the Deep Space Network (DSN) 34-m high efficiency Deep Space Stations (DSSs) located near Goldstone, California (DSS 15), Canberra, Australia (DSS 45), and Madrid, Spain (DSS 65). The tracking schedule includes one pass of data for each station per week. The tracking passes are started with DSS 15 on the first day, DSS 45 on day 4 and DSS 65 on day 6. After each station makes one pass, six passes (days) are skipped before the next pass at that station is initiated. Thus, DSS 15 will next track on day 7, DSS 45 on day 10 and DSS 65 on day 12. This pattern is repeated until the end of the considered portion of the trajectory. The interval between data points is 10 min with range and Doppler data collected at the same time. The minimum elevation angles are 50 deg for DSS 15 and DSS 65 and 30 deg for DSS 45. Data points for times when the elevation angle is smaller than these values are rejected. All data points that meet the requirements for the day of the pass, and the minimum elevation angle are included in the data set. These criteria were set to simulate the specified tracking schedule on one 4-h pass per week at each tracking station during interplanetary cruise.[4] Following this schedule, about 1250 range and 1250 Doppler measurements are available over the 105-day interplanetary cruise phase.

III. Covariance Analysis

The reduction of the estimation errors in the navigation problem is an area of study that has received considerable attention in recent years. One method of improving navigation accuracy is the use of advanced data types, such as very long baseline interferometry. The

drawback to using advanced data types is their expense resulting from extensive antenna time requirements and the use of multiple DSN sites simultaneously. For this reason, an effort has been directed at improving the navigation techniques using radio Doppler and ranging data collected using NASA's DSN.[1] The main attraction of these conventional data types is that they are routinely collected in tracking, telemetry, and command operations. For example, radio Doppler data are a free by-product of the communication link. Another advantage of conventional data types is their long history of use in tracking. This is important since the measurement error models are well developed because of the large set of data from several decades of missions.

To improve the navigation accuracy using conventional data types, it is desirable to determine the significant error sources that contribute to the total estimation error on a particular mission. Once the most significant error sources have been identified, more detailed work on those specific error sources can be completed with a goal of reducing their contribution to the overall error. This may be accomplished in many ways, such as improving the mathematical models based on past experience or by using data at different frequencies to reduce frequency dependent errors.

The method used to identify the major error contributors is the so-called linear covariance analysis.[5] Covariance analysis can be used to study changes in filter performance resulting from configuration changes in the filter. Examples include studying the effects of unestimated parameters and using incorrect a priori statistics on the overall state estimation error.[6] An error budget can be developed that catalogs the contribution of a particular error source or error source group to the total navigation uncertainty. The error budget identifies the most significant error sources for further study. A result easily obtained from the error budget tables is the sensitivity of the filter to variations in the input parameters. The error groups considered here consist of spacecraft accelerations resulting from solar radiation pressure and small nongravitational accelerations (NGA) (because of gas leaks, thruster misalignment, etc.), tracking station position errors, refraction resulting from the troposphere and ionosphere, and errors in the Earth orientation [pole motion and Earth rotation angle ($UT1$) errors]. These errors are the major contributors to the estimation error in interplanetary orbit determination.[7]

The models and values assumed for the error sources can be found in Table 2. Most are modeled as first-order Gauss–Markov random processes. The exceptions are the spacecraft state, with no associated process noise parameters, and the station locations, which are modeled as random biases with the variances shown in Table 2. The solar pressure model includes the symmetry of the spacecraft and the effect of the solar panels and reflects a 5% uncertainty in the model parameters. The NGA approximate small unmodeled forces in each of the three coordinate directions resulting from gas leaks and attitude maintenance activity. The models are based on the Mars Pathfinder operation plan.[4]

A. Error Budget Calculations

In general, the error budget is a summary of the contributions of all error sources that affect the filter estimate at a specific time, whether modeled explicitly or not. In this part of the study, it is assumed that the filter model and the truth model are the same. This implies that the filter model is an exact representation of the real world, which is not the case in actual application. However, it was desired to limit the modeling differences to parameters that could be controlled by the user for this study.

The models used in the covariance analysis are the same as the models used in the simulations of the interplanetary tracking with the following exceptions. The covariance analysis included gravitational effects from all planets and the moon, whereas the simulation results include only central body gravity. In addition, light time corrections were made in the covariance analysis that were neglected in the simulation results. Thus, the covariance analysis results are based on a more accurate model than was used in the simulation. An area for future study is to increase the fidelity of the simulations to match the models used in the covariance analysis.

Error budgets were developed for the Mars Pathfinder interplanetary cruise scenario and data schedule described earlier for Doppler and range data sets. The statistics for the orbit determination errors at the end of the tracking were propagated to the nominal time of Mars encounter and expressed in terms of the B-plane coordinate frame.[8] This coordinate frame, also known as the aiming plane, is defined by unit vectors $\boldsymbol{S}$, $\boldsymbol{T}$, and $\boldsymbol{R}$. The vector $\boldsymbol{S}$ is parallel to the spacecraft velocity vector relative to the target planet (Mars) at the time of entry into the target planet's gravitational sphere of influence, the vector $\boldsymbol{T}$ is perpendicular to the target planet equatorial plane and the vector $\boldsymbol{R}$ is such that the three unit vectors form a right-handed coordinate system. The miss vector $\boldsymbol{B}$ is the aim point for planetary encounter and lies in the $\boldsymbol{T}$–$\boldsymbol{R}$ plane. The miss vector would be the point of closest approach to the target planet if the target planet did not deflect the flight path of the spacecraft (i.e., the planet had no mass).

The statistics are presented as a 1-σ uncertainty of the miss vector resolved into miss components $\boldsymbol{B} \cdot \boldsymbol{R}$ (normal to the target planet equatorial plane) and $\boldsymbol{B} \cdot \boldsymbol{T}$ (parallel to the target planet equatorial plane), and a 1-σ uncertainty in the linearized time of flight (LTOF). The LTOF specifies the time of flight to encounter (point of closest approach) if the magnitude of the miss vector were zero and defines the time from encounter. To convert the LTOF to a distance, the hyperbolic approach velocity is required. For the Mars Pathfinder mission scenario, the hyperbolic approach velocity is 5.52 km/s. The miss vector, or the distance from the center of Mars where the spacecraft crosses the target plane, is 4550 km oriented 201.8 deg clockwise from the $\boldsymbol{T}$ axis. Plots of dispersion ellipses in the B plane are made for each case to illustrate the contributions of each error source to the overall error. More detailed information on the covariance analysis can be found in Burkhart et al.[9]

Table 2 Filter and truth model parameters (one way)

Name	A priori σ	Steady-state σ	Time constant, days
Spacecraft state	10 km, 1 cm/s	——	——
Solar radiation pressure			
Radial, G_r	5% (=0.07)	5%	60
Transverse, G_x/G_y	5% (=0.02)	5%	60
NGA, 10^{-12} km/s^2	0.7	0.7	7
Station locations			
Spin axis, cm	10	——	——
z height, cm	10	——	——
Longitude, cm	10	——	——
Pole orientation	10 cm (17 nrad)	10 cm	2
Rotation period	15 cm (0.3225 ms)	15 cm	1
Zenith troposphere (wet, each station)	5 cm	5 cm	0.1
Zenith ionosphere (wet, each station)	3 cm (0.5 el/m^2)	3 cm	0.2
Measurement noise			
Range	70 cm	——	——
Doppler	0.01 mm/s	——	——

Table 3 Error budget: Doppler measurements

Error source	$\boldsymbol{B} \cdot \boldsymbol{R}$, km	$\boldsymbol{B} \cdot \boldsymbol{T}$, km	LTOF, s
Epoch state	0.001	0.005	0.003
Solar radiation pressure parameters	10.692	10.454	6.829
NGA	18.252	13.633	2.822
Ionosphere	1.917	1.297	0.189
Troposphere	5.625	4.315	0.577
Station locations	5.263	4.484	0.534
Earth orientation	9.121	6.648	1.031
Measurement noise	7.102	5.542	0.751
RSS total	25.379	20.260	7.542

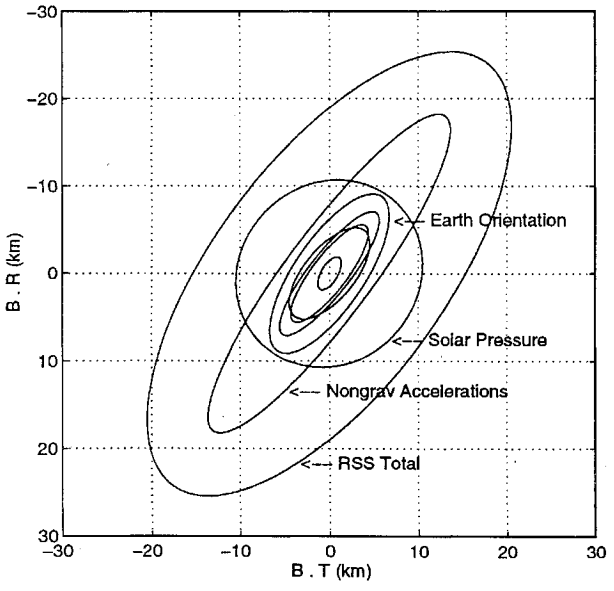

Fig. 2 Aiming plane dispersions (1-σ): Doppler data.

The encounter plane error ellipse requirements (1-σ) are 17 km for $\boldsymbol{B} \cdot \boldsymbol{R}$, 6.2 km for $\boldsymbol{B} \cdot \boldsymbol{T}$ and 7 s for LTOF, with the error ellipse oriented at 111 deg (Ref. 4).

B. Doppler-Only Case

The error budget results for the Doppler-only case are shown in Table 3. These results are the magnitudes of the B-plane dispersions about the nominal aim point for planetary orbit insertion for each filter (truth) model error source (in a root-mean-square sense) and for the total filter error. The Doppler case shows that the $\boldsymbol{B} \cdot \boldsymbol{R}$ component of the miss vector is determined to about 25 km and the $\boldsymbol{B} \cdot \boldsymbol{T}$ component of the miss vector is determined to about 20 km. The LTOF is determined to about 7 s (about 42-km uncertainty in position).

The plot of the 1-σ aiming plane dispersion ellipses for the Doppler-only case is shown in Fig. 2. The ellipses shown include the total filter result (all error sources) and the ellipse for each error source individually. The semimajor axis of the filter error ellipse is almost perpendicular to the line connecting the aim point (the origin of the plot) and the center of Mars. The largest contributors to the overall error are the solar pressure, the NGA, and the Earth orientation parameters.

C. Range-Only Case

The error budget results for the range-only case are shown in Table 4. For this case, the $\boldsymbol{B} \cdot \boldsymbol{R}$ component is determined to about 26 km and the $\boldsymbol{B} \cdot \boldsymbol{T}$ component is determined to about 17 km. The LTOF is determined to about 0.6 s (approximately 3 km). From the geometry of the trajectory (see Fig. 1) it can be seen that the Earth–spacecraft range component lies in the plane including the $\boldsymbol{B} \cdot \boldsymbol{T}$ and LTOF directions. The contribution to the overall error budget resulting from most of the error sources is much smaller than the contribution resulting from the measurement noise. Most of the errors in this case will probably be masked by the measurement noise when adaptation is attempted.

Table 4 Error budget: range measurements

Error source	$\boldsymbol{B} \cdot \boldsymbol{R}$, km	$\boldsymbol{B} \cdot \boldsymbol{T}$, km	LTOF, s
Epoch state	4.76e−4	3.52e−4	5.38e−6
Solar radiation pressure parameters	8.858	7.179	0.222
NGA	19.615	12.667	0.369
Ionosphere	0.220	0.147	0.007
Troposphere	7.001	4.127	0.097
Station locations	5.075	4.162	0.170
Earth orientation	1.652	1.041	0.057
Range biases	4.549	1.776	0.140
Measurement noise	11.593	5.836	0.321
RSS total	26.397	16.880	0.591

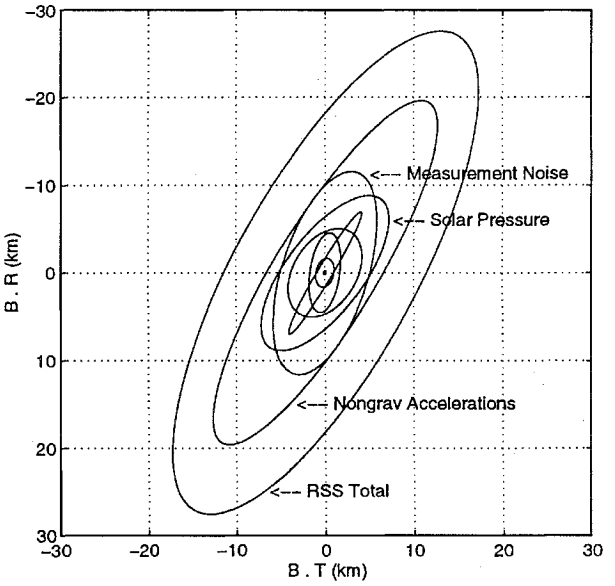

Fig. 3 Aiming plane dispersions (1-σ): range data.

The plot of the error ellipses for the range-only case appears in Fig. 3. The biggest contributors to the overall error are the NGA and measurement noise, with smaller effects resulting from the solar pressure and troposphere similar in magnitude. Earth orientation is much less important than for the Doppler-only case, and the measurement noise contributes more to the range-only errors than to the Doppler-only case. In addition, the NGA contribute more to the overall error for this case than the Doppler-only case. The measurement noise ellipse is oriented slightly differently than the other major error ellipses, which is also different from the Doppler-only case, where the measurement error ellipse was oriented closer to the major error sources. As before, the semimajor axis of the error ellipse is nearly perpendicular to the aim point–Mars equator line.

From the results obtained, it is clear that the goal of reducing the overall navigation error can be best achieved by concentrating effort on spacecraft accelerations (solar pressure and random NGA) and measurement noise. These errors will be the focus of the adaptive filtering.

IV. Adaptive Filtering Approaches

An implicit assumption in the Kalman filter is that all of the system parameters, including the state transition matrix, the measurement partial derivatives, and the process and measurement noise matrices, are known. In general, this is not the case. Often there are parameters not included in the filter model that influence the measurements. This results in a modeling mismatch between the filter and the measurements, which affects the state transition matrix and the measurement partials. In addition, the process noise and measurement noise

matrices are rarely precisely known. For these reasons, it may be desirable to apply an adaptive filtering scheme to the problem at hand.

The general problem to be solved is described by

$$z_{i+1} = \Phi_i z_i + u_i$$

$$y_i = H_i z_i + v_i$$

where z_i is the state vector, Φ_i the state transition matrix, u_i the process noise vector, v_i the measurement noise vector, and H_i the measurement matrix. Both u_i and v_i are uncorrelated zero-mean Gaussian white noise sequences, with

$$E\{u_i\} = 0, \qquad E\left\{u_i u_j^T\right\} = Q\delta_{ij}$$

$$E\{v_i\} = 0, \qquad E\left\{v_i v_j^T\right\} = R\delta_j$$

where Q is a nonnegative definite matrix and R is a positive definite matrix, both with unknown true values. The standard filtering problem is to estimate z_i based on the observation set $y_i^* = \{y_1, y_2, \ldots, y_i\}$, where the estimated values will be denoted $\hat{z}_i$. In this case, the discrete Kalman filter is used:

$$\hat{z}_{i+1}^{(-)} = \Phi_i \hat{z}_i^{(+)}$$

$$P_{i+1}^{(-)} = \Phi_i P_i^{(+)} \Phi_i^T + Q$$

$$\hat{z}_i^{(+)} = \hat{z}_i^{(-)} + K_i\left(y_i - H_i \hat{z}_i^{(-)}\right)$$

$$K_i = P_i^{(-)} H_i^T \left(H P_i^{(-)} H_i^T + R\right)^{-1}$$

$$P_i^{(+)} = (I - K_i H_i) P_i^{(-)}$$

where K_i is the Kalman gain and $\nu_i = y_i - H_i \hat{z}_i^{(-)}$ is the measurement residual with covariance $H P_i^{(-)} H_i^T + R$. This solution is optimal based on exact knowledge of Q and R. Since this is not the case here, an adaptive filter will be used to help determine Q and R.

A. Evaluation of Adaptive Methods

Based on the discussion presented by Mehra[10] in 1972, adaptive filtering methods can be divided into four groups: maximum likelihood, correlation, covariance matching, and Bayesian. Covariance matching techniques will not be discussed here.

A literature survey revealed several potential solutions to our problem. Computer experiments were conducted on the methods that showed the most promise.[11] A brief summary is presented here. Of the maximum likelihood methods, the one with a history in orbit determination was proposed by Meyers and Tapley.[12] However, this approach did not offer a significant improvement over current practice. Many correlation methods exist, but the most well known was proposed by Mehra.[13] However, correlation methods are better suited to time-invariant problems. Attempts to extend this approach to time-varying problems have not been successful.[14] The Bayesian approach that is perhaps the most well known is that originally formulated by Magill.[3] This method is known as simply the Kalman filter bank or the MMEA, shown in Fig. 4.[15] The approach is to implement a bank of Kalman filters, each modeled with different values of a finite unknown parameter set. The method, in its original form, computes the weighted sum of the estimates from each filter to determine the optimal adaptive estimate.

The main reason the Kalman filter bank approach was selected here is that it solves the orbit determination problem quite well. The proposed methodology is also a practical extension to current navigation practices for interplanetary spacecraft. The cost of integrating this approach with the current operational enhanced Kalman filter is minimal. All that is required from the filter are pre-update measurement residuals and the covariance associated with these residuals at each data point, which are already computed by the Kalman filter. The assumptions that are required for application of the filter bank are the same that govern the use of a single Kalman filter. Thus, if the problem is formulated such that the Kalman filter is applicable, then the filter bank approach can be used without modification.[16]

In addition, the filter bank approach has been shown to be a practical algorithm in solving real-world problems.[17–19] One important problem that can be solved most effectively using the Magill filter bank is that of hypothesis testing, which is to choose from among a finite set of filters the optimal filter in the bank.[15,16] In this use, the output of interest is the weight computed for each filter in the bank. The Kalman filter bank implemented in this study is utilized as a hypothesis tester.

The Kalman filter bank will allow the analyst to model several filters simultaneously and directly compare the results automatically. The filter bank will determine which filter is operating optimally (where optimal is precisely defined later) with respect to the measurement data, thus helping the process of selecting the filter parameters. For the case where the process and/or measurement noise

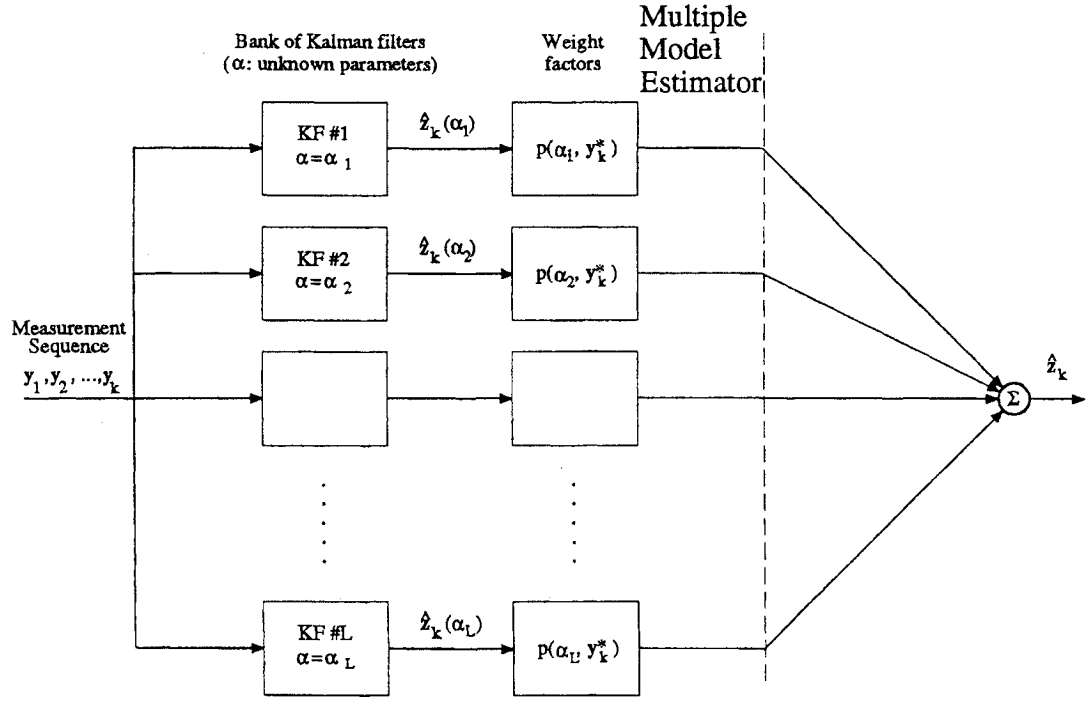

Fig. 4 Weighted sum of Kalman filter estimates.

profile changes, the filter bank can deselect a given filter and choose a different filter that more closely matches the current environment. In this way, in addition to the establishment of a systematic method to choose the operational filter parameters and to detect environmental changes, the orbit determination process can be completed with fewer team members, while potentially increasing the accuracy and timeliness of the results.

B. Adaptive Kalman Filter Bank Development

The problem to be solved may be stated as follows. An estimate is desired for a sampled-data, Gaussian process, which may be corrupted by additive noise, such that the estimate minimizes some performance measure. The observed process is a function of some unknown parameter vector α, which is a member of a finite set of known parameter vectors.[3]

Assume that the parameter vector α is a random variable that may or may not be Gaussian. This implies that α is an unknown constant for a specific sample run, but has a known statistical distribution. The optimal estimate $\hat{z}_k$ is a weighted sum of the individual Kalman filters, with each filter operating with a different value of α. The weighted sum, for L Kalman filters, is given by

$$\hat{z}_k = \sum_{i=1}^{L} \hat{z}_k(\alpha_i) p\left(\alpha_i \mid y_k^*\right) \tag{1}$$

where $p(\alpha_i \mid y_k^*)$ is the discrete probability for α_i conditioned on the measurement sequence y_k^*. The problem now is reduced to the determination of the weight factors $p(\alpha_1 \mid y_k^*)$, $p(\alpha_2 \mid y_k^*)$, etc. As the measurement process evolves, the weights change recursively. As more measurements are processed, the knowledge of the state and the unknown parameter α will increase. If as time progresses it is possible to learn which stochastic process is observed, then it is reasonable to expect the optimal estimator to converge to the appropriate filter for that process. In terms of the block diagram in Fig. 4, the weighting coefficient for the true filter will converge to one, whereas all of the rest will converge to zero.[3,20]

The weighting factors $p(\alpha_i \mid y_k^*)$ are the adaptive features of this estimator.[3] Using Bayes' rule, the weights are computed via

$$p\left(\alpha_i \mid y_k^*\right) = \left[\frac{p\left(y_k^* \mid \alpha_i\right) p(\alpha_i)}{\sum_{j=1}^{L} p\left(y_k^* \mid \alpha_j\right) p(\alpha_j)}\right], \qquad i = 1, 2, \ldots, L \tag{2}$$

The values for $p(\alpha_i)$ are assumed known, so all of the terms in this relation are known except for $p(y_k^* \mid \alpha_j)$. To compute the value for $p(y_k^* \mid \alpha_j)$, the processes x and y will be assumed to be Gaussian. In addition, the measurement sequence y_k^* will be assumed to be a sequence of scalar measurements $y_0, y_1, \ldots, y_k$. When these conditions are applied, the result is

$$p\left(y_k^* \mid \alpha_j\right) = \frac{1}{\sqrt{2\pi\left(H_k P_k^- H_k^T + R_k\right)}} \times \exp\left[-\frac{1}{2}\frac{\left(y_k - H_k \hat{z}_k^-\right)^2}{\left(H_k P_k^- H_k^T + R_k\right)}\right] p\left(y_{k-1}^* \mid \alpha_j\right) \tag{3}$$

In general, $p(y_k^* \mid \alpha_j)$ will be different for each filter in the bank.

In the Mars Pathfinder problem, only the a posteriori probabilities $p(\alpha_i \mid y_k^*)$ for each hypothesis are computed by the filter bank. As the filter bank processes data, the weighting factor for the best filter will increase while the other weighting factors decrease.[15] For this problem, the Kalman filters are assumed to have an unknown measurement noise variance, in addition to possibly unknown process noise parameters. All other parameters and models between the filter and the environment are the same. Thus the MMEA will be determining the filter with the parameters that are the closest to the values from the environment, as determined from the measurements.

V. Results

Results from several sets of cases are shown. The first set of results are for range cases where all noise parameters are included in the filter, but only a selected group of parameters are adaptively determined. The case presented here is for adaptation of measurement noise and NGA parameters. In addition to the range cases, several cases where Doppler data are processed are shown. The final case shown involves a change in the nongravitational parameter during tracking. Range data are utilized in this study along with a high-gain antenna, which reduces the random noise component of the noise profile. This allows the Kalman filter bank to run over a larger set of data.[11]

The filter model parameters and assumptions are described in the covariance analysis discussion. The weighting coefficients for each filter in the bank are presented as a function of time, along with the estimates, computed error covariances, and true values in the encounter plane. All error ellipses plotted for the filter bank results

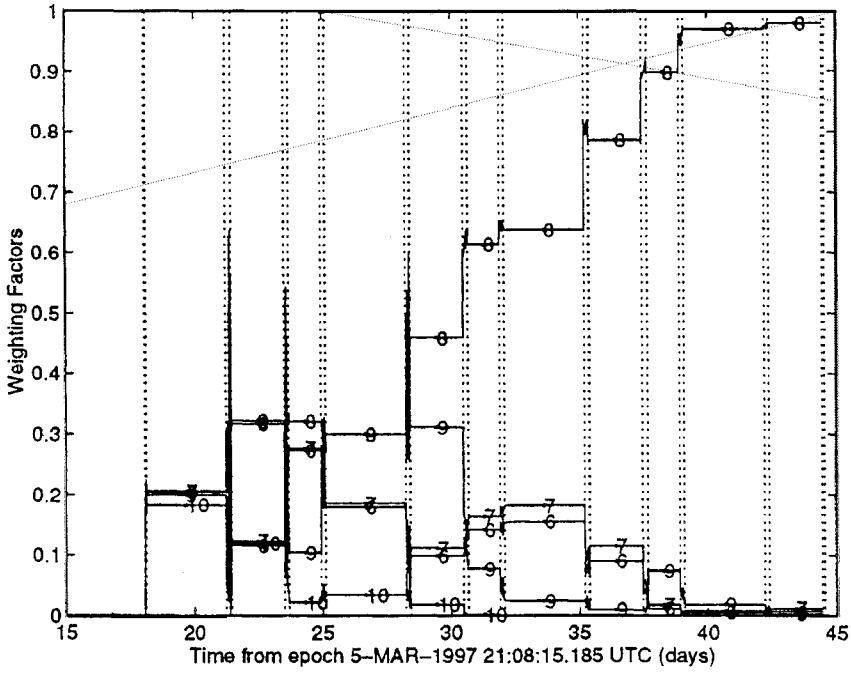

Fig. 5 Weighting coefficients: measurement and NGA parameters adapted (range).

show 1-σ errors. The ellipses for the simulation results are oriented differently from those for the error budget analysis because of the model differences discussed earlier.

Results are not presented in this paper, because of space limitations, for the residuals and error covariances for the individual filters. These are useful in determining how well the filters are performing. The results obtained (but not shown here) show that the filter performance matches the computed weighting factors. In other words, filters with higher weights performed better than those with smaller weights.

A. Range Case

The first case considered adapts the NGA parameters and the measurement noise parameter. A bank of 15 filters is set up with the scaling from the nominal values shown in Table 5. The filter numbers are determined as shown in the table. For example, filter 14 has a measurement noise that is 10 times the nominal value and a NGA steady-state variance that is 5 times the nominal value.

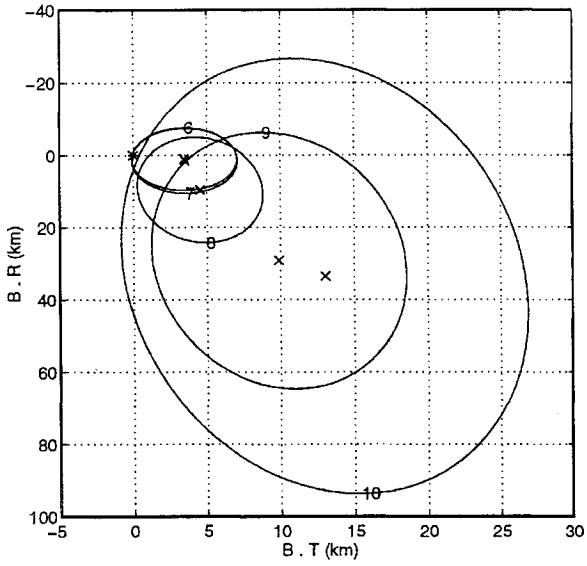

Fig. 6 Encounter results: measurement and NGA parameters adapted (range).

The weighting factors for this scenario are plotted in Fig. 5. This plot shows nonzero weights for filters 6–8. The weight for filter 8 is nearly unity, whereas the other filters have negligible weights. The filters in the bank that do not have the correct measurement noise parameter are eliminated quickly by the MMEA. The remaining data are used to differentiate the process noise values from among the filters with the correct measurement noise parameter.

The encounter plane estimates and covariances for filters 6–10 are shown in Fig. 6. For this case, filters 6 and 7 appear to be quite close to the truth. Filter 8, with a slightly higher weight and the correct filter, had slightly worse estimates. Since these results are based on a single realization of the random processes, Monte Carlo analysis with different realizations of the random processes was conducted to verify the expected results. The Monte Carlo results are presented in Burkhart.[11]

B. Doppler Case

The Doppler case adapts the NGA parameters and the measurement noise parameter. A bank of 15 filters is set up with the scaling from the nominal values as shown in Table 5 for the range case.

The weighting factors for this scenario are plotted in Fig. 7. This plot shows nonzero weights for filters 11–15. The weight for filters 11 and 12 are approximately 0.4, whereas filter 13 has a weight near 0.25 and filters 14 and 15 have weights of about zero. As before, the correct filter is filter 8. Thus, for this case, the filter does not converge to the correct filter. These results for the Doppler case are not as conclusive as for the range case. Problems with the formulation of the Doppler measurement resulting from linearization and the differenced range formulation are apparent from the results. The filter chosen by the filter bank has similar or smaller process noise and larger measurement noise compared to the environment.

Table 5 Scaling factors: measurement and NGA parameters

NGA scaling	Filter number		
0.1	1	6	11
0.2	2	7	12
1.0	3	8	13
5.0	4	9	14
10.0	5	10	15
	0.1	1.0	10.0
	Measurement noise scaling		

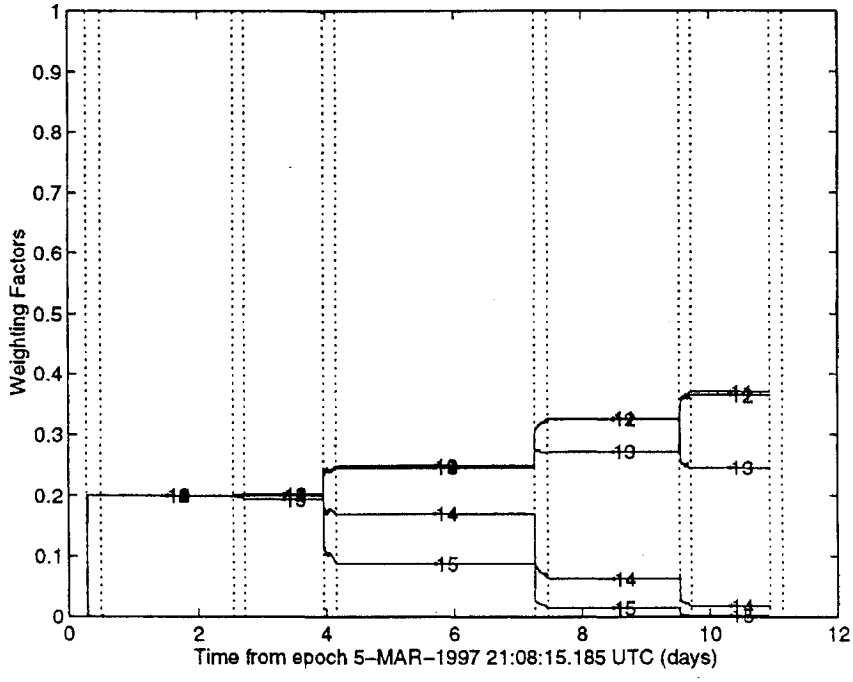

Fig. 7 Weighting coefficients: measurement and NGA parameters adapted (Doppler).

The encounter plane estimates and covariances for filter 8 and filters 11–15 are shown in Fig. 8. For this case, filter 8 appears to be the best filter.

C. Study of Noise Parameter Variations

The final run presented involves simulated range data with a change in the NGA steady-state variance after approximately half of the tracking segment is complete. The parameter change represents a possible valve leak after a TCM or some other change in the force profile of the spacecraft. This variance is assumed constant for the first part of the tracking. After 62 days of tracking, or just after the Mars Pathfinder TCM 2, the parameter is changed to a new constant value. This situation represents the effect of a thruster leaking after it is fired for the TCM, a leak in a fuel line, or some other phenomena related to a thruster malfunction. The process noise term is scaled by 10, which corresponds to scaling the NGA variance by $\sqrt{10}$. The scaling was chosen to be such that the correct filter (after the variance change) is no longer part of the bank of 15 filters (see Table 5). In this way, the case will illustrate that the bank will converge to the filter operating the closest to the data's noise profile. All error sources are included in the simulation.

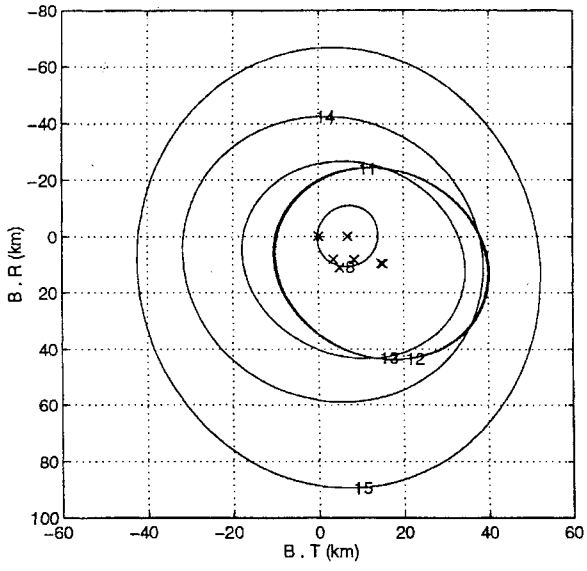

Fig. 8 Encounter results: measurement and NGA parameters adapted case (Dopper).

The weighting factors for each filter are shown in Fig. 9. For the first 60 days of tracking, the filter is converging to filter 8, which is the correct filter. After the change in the variance, the filter quickly selects filter 9, which has nominal values for all variances except a scaling on the NGA of 5. It is thus shown that the bank is able to detect changes resulting from unmodeled thruster variations.

VI. Conclusions

The adaptive estimation solution described in this work solves the orbit determination problem very effectively given the real-world constraints. The adaptive filter can be used as an effective tool to assist the navigation engineer in selecting filter parameters, thus allowing a closer match of the filter parameters to the true values, leading to a potentially more accurate navigation solution. In addition, this method requires fewer hours of processing and analysis and allows a smaller group of analysts to determine accurate navigation solutions. More importantly, the long-term objective of this study is to develop an adaptive filtering methodology that can be used for processing of actual mission data. It has been shown in this study that this objective is achievable.

Results for the range cases show that the Magill enhanced Kalman filter bank chooses the filter with the same parameters as the simulated data. Cases where there was no clear winner were shown to have several filters with nonzero weights and similar performance. Smaller error sources, as determined by covariance analysis, are more difficult to determine, leading to selection of no single filter, but rather several with similar performance. Based on these results, the filter bank will be a useful tool in the tuning process for the operational filter. In addition, the bank is useful for the determination of changes in the tracking data, giving a warning of potential problems such as a thruster malfunction or some other change in the acceleration profile of the spacecraft.

Results for the Doppler cases are less conclusive. One problem with this formulation of the Doppler measurement is the effect of roundoff errors resulting from the linearization and the differenced range formula. For example, the range values are on the order of 10^8 km. The measurement noise on the Doppler measurement is 0.01 mm/s, or 10^{-8} km. The difference is 16 digits, or near the numerical limits of a 64-bit number. In addition, the differenced range formulation implemented in the partial derivatives and the data generation may be susceptible to differences because of Earth rotation from the start to the end of the tracking pass. One way to

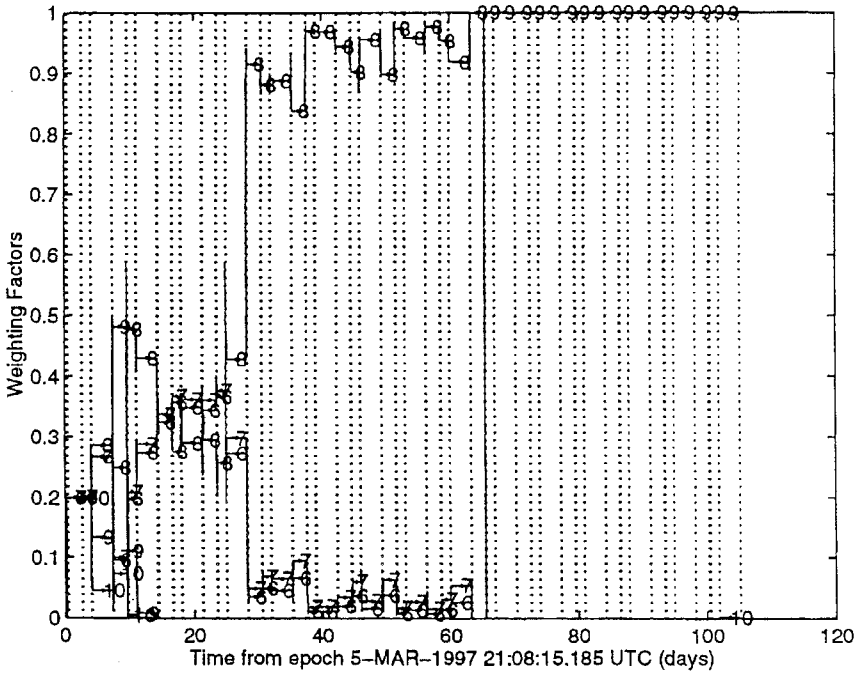

Fig. 9 Weighting coefficients: NGA parameter change (high-gain-antenna range).

address these problems is to implement a more theoretically correct version of the range rate measurement. In addition, an extended Kalman filter, which does not involve a linearization about a reference trajectory, may help this problem as well. The Doppler results, in general, show that filters with larger measurement noise are chosen, while the other filters have zero weights. In most cases, the filters with correct or smaller process noise are chosen, as for the range case.

A next step is implementation of the filter bank for use in processing actual mission data. The proposed method could be used by the navigation team members making the individual runs to systematically eliminate incorrect filter models. This could be completed by several individuals independently, with comparison of results after processing is complete. The development of an extended Kalman filter capable of processing real data is under way, and the Mars Pathfinder problem will be one of the first cases tested.

One additional advantage is the obvious parallel computing possibilities with this approach. This approach can be implemented using search methods (such as genetic algorithms[21]) to update the filter bank for operation in an iterative fashion. These genetic algorithms can be implemented easily using the filter bank and can be implemented in a parallel processing environment.[22]

The Kalman filter bank is a method that has a successful history in real-time applications such as power system fault detection, image processing, and terrain-height correlation for helicopter navigation. It has been shown here to also have application in interplanetary orbit determination.

Acknowledgments

This study was partially funded under NASA Contract 959577 with the Jet Propulsion Laboratory, California Institute of Technology. The authors would like to thank Jeff Estefan, Vincent Pollmeier, Sam Thurman, and Lincoln Wood of the Jet Propulsion Laboratory for their contributions to this study.

References

[1]Estefan, J. A., Pollmeier, V. M., and Thurman, S. W., "Precision X-Band Doppler and Ranging Navigation for Current and Future Mars Exploration Missions," *Advances in the Astronautical Sciences*, edited by J. Teles and M. V. Samii, Vol. 84, Pt. 1, Univelt, San Diego, CA, 1993, pp. 3–16.

[2]Bhaskaran, S., Thurman, S. W., and Pollmeier, V. M., "Demonstration of a Precision Data Reduction Technique for Navigation of the Galileo Spacecraft," *Advances in the Astronautical Sciences*, edited by J. E. Cochran Jr., C. D. Edwards Jr., S. J. Hoffman, and R. Holdaway, Vol. 87, Pt. 2, Univelt, San Diego, CA, 1994, pp. 785–798.

[3]Magill, D. T., "Optimal Adaptive Estimation of Sampled Stochastic Processes," *IEEE Transactions on Automatic Control*, Vol. AC-10, No. 4, 1965, pp. 434–439.

[4]Kallemeyn, P., "Pathfinder Project Navigation Plan–Critical Design Review Version," Jet Propulsion Lab., JPL Document D-11349 (Internal Document), California Inst. of Technology, Pasadena, CA, July 1994.

[5]Gelb, A., *Applied Optimal Estimation*, MIT Press, Cambridge, MA, 1974.

[6]Bierman, G. J., *Factorization Methods for Discrete Sequential Estimation*, Academic, New York, 1977.

[7]Jordan, J. F., Madrid, G. A., and Pease, G. E., "Effects of Major Error Sources on Planetary Spacecraft Navigation Accuracies," *Journal of Spacecraft and Rockets*, Vol. 9, No. 3, 1972, pp. 196–204.

[8]Kizner, W., "A Method of Describing Miss Distances for Lunar and Interplanetary Trajectories," Jet Propulsion Lab., JPL External Publication No. 674, California Inst. of Technology, Pasadena, CA, Aug. 1959.

[9]Burkhart, P. D., Bishop, R. H., and Estefan, J. A., "Covariance Analysis of Mars Pathfinder Interplanetary Cruise," *Advances in the Astronautical Sciences*, edited by R. J. Proulx, J. J. F. Liu, P. K. Seidelmann, and S. Alfano, Vol. 89, Pt. 1, Univelt, San Diego, CA, 1995, pp. 267–285.

[10]Mehra, R. K., "Approaches to Adaptive Filtering," *IEEE Transactions on Automatic Control*, Vol. AC-17, No. 10, 1972, pp. 693–698.

[11]Burkhart, P. D., "Adaptive Orbit Determination for Interplanetary Spacecraft," Ph.D. Dissertation, Dept. of Aerospace Engineering and Engineering Mechanics, Univ. of Texas, Austin, TX, May 1995.

[12]Meyers, K. A., and Tapley, B. D., "Adaptive Sequential Estimation with Unknown Noise Statistics," *IEEE Transactions on Automatic Control*, Vol. AC-21, No. 8, 1976, pp. 520–523.

[13]Mehra, R. K., "On the Identification of Variances and Adaptive Kalman Filtering," *IEEE Transactions on Automatic Control*, Vol. AC-15, No. 2, 1970, pp. 175–184.

[14]Bélanger, P. R., "Estimation of Noise Covariance Matrices for a Linear Time-Varying Stochastic Process," *Automatica*, Vol. 10, May 1974, pp. 267–275.

[15]Brown, R. G., and Hwang, P. Y. C., *Introduction to Random Signals and Applied Kalman Filtering*, 2nd ed., Wiley, 1992, pp. 398–402.

[16]Brown, R. G., "A New Look at the Magill Adaptive Filter as a Practical Means of Multiple Hypothesis Testing," *IEEE Transactions on Circuits and Systems*, Vol. CAS-30, No. 10, 1983, pp. 765–768.

[17]Brown, R. G., and Hwang, P. Y. C., "A Kalman Filter Approach to Precision GPS Geodesy," *Navigation, Journal of the Institute of Navigation*, Vol. 30, No. 4, 1983, 1984, pp. 338–349.

[18]Mealy, G. L., "Application of Multiple Model Estimation to a Recursive Terrain Height Correlation System," *IEEE Transactions on Automatic Control*, Vol. AC-28, No. 3, 1983, pp. 323–331.

[19]Girgis, A. A., and Brown, R. G., "Adaptive Kalman Filtering in Computer Relaying: Fault Classification using Voltage Models," *IEEE Transactions on Power Apparatus and Systems*, Vol. PAS-104, No. 5, 1985, pp. 1168–1177.

[20]Hilborn, C. G., Jr., and Lainiotis, D. G., "Optimal Adaptive Filter Realizations for Sample Stochastic Processes with an Unknown Parameter," *IEEE Transactions on Automatic Control*, Vol. AC-14, Dec. 1969, pp. 767–770.

[21]Goldberg, D. E., *Genetic Algorithms in Search, Optimization, and Machine Learning*, Addison–Wesley, Reading, MA, 1989.

[22]Chaer, W. S., and Bishop, R. H., "Adaptive Kalman Filtering with Genetic Algorithms," *Advances in the Astronautical Sciences*, edited by R. J. Proulx, J. J. F. Liu, P. K. Seidelmann, and S. Alfano, Vol. 89, Pt. 1, Univelt, San Diego, CA, 1995, pp. 141–156.